Effects of excessive impregnation, magnesium content, and pyrolysis temperature on MgO-coated watermelon rind biochar and its lead removal capacity

Jingzhuo Zhang[1], Deyi Hou[1,*], Zhengtao Shen[1,2,*], Fei Jin[3], David O'Connor[1], Shizhen Pan[1,4], Yong Sik Ok[5], Daniel C.W. Tsang[6], Nanthi S. Bolan[7], Daniel S. Alessi[2]

[1] School of Environment, Tsinghua University, Beijing 100084, China

[2] Department of Earth and Atmospheric Sciences, University of Alberta, Edmonton T6G 2E3, Canada

[3] School of Engineering, University of Glasgow, Glasgow G12 8QQ, United Kingdom

[4] School of Chemical and Environmental Engineering, China University of Mining and Technology, Beijing 100083, China

[5] Korea Biochar Research Center, O-Jeong Eco-Resilience Institute (OJERI) & Division of Environmental Science and Ecological Engineering, Korea University, Seoul 02841, Republic of Korea

[6] Department of Civil and Environmental Engineering, The Hong Kong Polytechnic University, Hung Hom, Kowloon, Hong Kong, China

[7] Global Centre for Environmental Remediation, ATC Building, Faculty of Science and Information Technology, The University of Newcastle, Callaghan NSW 2308, Australia

***Corresponding author:**

Deyi Hou,

School of Environment,

Tsinghua University,

Beijing 100084, China

Tel. +86(10) 62781159; Fax: +86(10) 62781159

E-mail: houdeyi@tsinghua.edu.cn

&

Zhengtao Shen,

Department of Earth and Atmospheric Sciences,

University of Alberta,

Edmonton T6G 2E3, Canada.

Tel. +1(78) 07071868; Fax: +1(78) 07071868

E-mail: ztshennju@gmail.com

Abstract

MgO-coated watermelon rind biochar (MWRB) is a potentially highly-effective waste-derived material in environmental applications. This research aims to provide valuable insights into the optimization of the production of MWRB for superior environmental performance. It was found that the Mg content of the MWRB could be easily controlled by adjusting the Mg/feedstock mass ratio during excessive impregnation. The BET surface area was found to first increase and then decrease as the Mg content of the MWRB (produced at 600 °C) increased from 1.52% to 10.1%, with an optimal surface area of 293 m^2/g observed at 2.51%. Similarly, an optimum pyrolysis temperature of 600°C was observed in the range of 400-800 °C for a maximum surface area of the MWRB at a fixed Mg/feedstock ratio of 0.48% (resulting in MWRBs with Mg contents of 1.89-2.51%). The Pb removal capacity of the MWRB (produced at 600°C) increased with increasing Mg content, with a greatest Pb removal capacity of 558 mg/g found for the MWRB with the highest Mg content (10.1%), an improvement of 208% over the 181 mg/g Pb removal capacity of unmodified WRB produced at 600°C. The Pb removal capacity of the MWRB (produced with 1.89-2.51% Mg) was also discovered to increase from 81.7 mg/g (at 400 °C) to 742 mg/g (at 700°C), before dropping to 368 mg/g at 800 °C. These findings suggest that the MWRB can be more efficiently utilized in soil and water remediation by optimizing its synthesis conditions.

Keywords

Engineered/designer biochar; green/sustainable remediation; pyrolysis temperature; magnesium oxide; lead removal

1 Introduction

Heavy metals represent a widely distributed environmental concern (e.g., in soil and water) due to their presence in industrial emissions and consumer products (O'Connor et al., 2018a; Wang et al., 2019c; Zhang et al., 2018a). For example, lead (Pb) is a problematic soil and water contaminant worldwide, posing a significant hazard to human health, especially affecting the development of brain and nervous system children (Shen et al., 2018b; Wang et al., 2019b; Zhang et al., 2019). It was estimated in 2013 that 0.6% of the world's disease and approximately 853000 deaths were caused by Pb pollution (Shi et al., 2019). The development of engineered reactive materials is garnering much attention, as an ever improving approach to remediation (Kang et al., 2019; O'Connor et al., 2018b; Zhang et al., 2017b), in particular, biochar is seeing a growing interest in its use for heavy metal removal owing to its greener credentials in comparison to other energy-intensive technologies (e.g., electrokinetic remediation and soil washing) (Song et al., 2019).

Biochar, a carbon rich material, can be produced from various biomass feedstocks *via* pyrolysis in an oxygen limited environment. Because of its high surface area, alkalinity, abundant oxygen-containing functional groups, and high cation exchange capacity (CEC) (Ahmad et al., 2014; Inyang et al., 2016; Mohanty et al., 2018), biochar can be used as an effective sorbent for many heavy metals. Furthermore, biochar can be used to mitigate climate change by gathering carbon from atmosphere, or to enhance soil fertility by improving nutrient retention and moisture holding capacity (Tang et al., 2013; Yang et al., 2018). Therefore, biochar is increasingly regarded as a sustainable solution for water and soil remediation (Hou et al., 2018; O'Connor et al., 2018c; Song et al., 2019).

Although biochar has revealed good performance for a range of applications in water and soil remediation, it has not been universally effective (Chen et al., 2019b; Shen et al., 2018c; Shen et al., 2016). This means that biochars may need further improvement (engineered biochar) to reach remediation targets (O'Connor et al.,

2018b; Rajapaksha et al., 2016; Yao et al., 2013). Biochar can be engineered/modified through chemical, physical, impregnation, or magnetic approaches to improve its performance (Cao et al., 2018; Rajapaksha et al., 2016). Recently, MgO modified biochar, or MgO-biochar composite, has been found to be promising in environmental applications (Ling et al., 2017; Shen et al., 2019b; Zhang et al., 2012). For example, MgO coating was observed to significantly enhance the adsorption capacity of Cr^{6+} for sugarcane harvest residue biochar from 20.79 mg/g to 54.64 mg/g (Xiao et al., 2018). Likewise, MgO-coated corncob biochar was found to effectively immobilize Pb to reach Toxicity Characteristic Leaching Procedure (TCLP) regulatory levels when applied to a soil washing residue, while the original corncob biochar was ineffective (Shen et al., 2019b).

In order to coat MgO on biochar, $MgCl_2$ is typically applied to the feedstock as a pre-treatment before pyrolysis (Jellali et al., 2016; Jung and Ahn, 2016; Li et al., 2016; Ling et al., 2017; Shen et al., 2019b). Two methods have been used for the pre-treatment: “ultrasonic impregnation” and “excessive impregnation” (Wang et al., 2015c; Zhu and Zhang, 2008; Zhu et al., 2015). With the ultrasonic impregnation method the remaining $MgCl_2$ may produce large aggregates during thermal decomposition under pyrolysis, which may result in the heterogeneity of magnesium (Mg)-containing minerals on biochar and the blockage of biochar pores after synthesis (Shen et al., 2019b). In the excessive impregnation method the excess $MgCl_2$ solution is removed by filtration after thorough mixing, therefore this approach has been favored. Excessive impregnation may improve in the homogeneity of $MgCl_2$ mixing and the uniform distribution of Mg-containing minerals in biochar after pyrolysis. However, the amount of $MgCl_2$ adsorbed on the feedstock remains unclear, bringing difficulty in controlling the final Mg content in biochar.

The enhancement of MgO coating for biochar mainly involves enhanced surface area and pore structure fashioned by $MgCl_2$ activation, and increased buffering capacity owing to the MgO content (Li et al., 2016; Shen et al., 2018a). These enhanced

properties result in biochar with better performance in environmental applications. It was observed that MgO coating (Mg content of 11.96%) greatly increased the surface area of corncob biochar from 0.07 to 26.56 m^2/g (Shen et al., 2019b). In comparison, the surface areas of MgO-coated magnetic sugarcane harvest residue biochars with Mg contents from 2.12% to 20.47% were examined, and it was observed that the surface area of the engineered biochar decreased with increasing Mg content from 118 to 27.2 m^2/g. These suggest that the surface area of MgO-coated biochar is closely related to its Mg content, as a result of the trade-off between fashioned pore structure by $MgCl_2$ activation and pore blockage by coated MgO.

The maximum pyrolysis temperature also plays an important factor determining the properties of MgO modified biochar. The temperature will determine the degree to which the $MgCl_2$ solution will thermally decompose, and the amount of MgO produced. The heating temperature also influences the formation of intermediate products (Huang et al., 2011), and the purity, crystal structure, and reactivity of MgO (Huang et al., 2011; Wang et al., 2019a). In addition, the properties of biochar itself are also significantly affected by pyrolysis temperature (Shen et al., 2019a; Suliman et al., 2016; Zhao et al., 2018).

In view of these considerations, the effects of excessive impregnation, Mg content, and pyrolysis temperature on the characteristics of MgO-coated watermelon rind biochar (MWRB) were investigated. Watermelon rind was used as the feedstock based on pre-trial investigations, watermelon rind biochar (WRB) revealing significantly higher adsorption capacities for heavy metals among the different fruit wastes tested (watermelon rind, pomelo peel, banana peel, mandarin orange peel, and sugarcane peel). As a common and abundant agricultural by-product, watermelon rind is rich in ash and carbohydrates, giving WRB the potential to have excellent performance in soil and water remediation (Lam et al., 2016). However, the surface area of WRB was found to be relatively small. The objective of this work is to find out the optimal synthesis parameters to produce MWRB with the highest surface area

and most outstanding performance in heavy metal removal.

2 Materials and methods

2.1 Synthesis of MgO modified watermelon rind biochar

The watermelon rind was obtained from Zhaolanyuan Canteen, Tsinghua University, Beijing, China. The watermelon rind was oven dried at 80°C for 48 h, and then crushed and sieved through #20 mesh (≤ 0.83 mm). The feedstock was pretreated by $MgCl_2$ using excessive impregnation (Wang et al., 2015c), involving 10 g of watermelon rind added to 200 mL of $MgCl_2$ solution, and agitated at 240 rpm for 24 h by magnetic stirrer. After stirring, the treated feedstock and excess $MgCl_2$ solution were separated by vacuum filtration. The filtration residue was oven dried at 80°C for 24 h, crushed and sieved through #40 mesh (≤ 0.83 mm).

The dried mixture was pyrolyzed in a muffle furnace with the heating rate of 10°C/min from room temperature to 600°C (or designated highest temperatures for the temperature-dependence study), and maintained for 1 h (Shen et al., 2019b; Wang et al., 2015b). The produced biochar was washed with deionized water three times, and oven dried at 80°C for 24 h. The dried biochar was sieved (≤ 0.38 mm) and stored in sealed sample bags.

2.2 Effects of excessive impregnation, magnesium content, and pyrolysis temperature

To assess if the Mg content of MWRB could be controlled, various $MgCl_2$ concentrations were used (0.005, 0.01, 0.05, 0.1, and 0.3 M), corresponding to Mg/feedstock mass ratios of 0.24%, 0.48%, 2.4%, 4.8%, and 14.4%.

In order to assess the effect of pyrolysis temperature on the properties of MWRB, it was produced at 400, 500, 600, 700, and 800°C with the $MgCl_2$ solution concentration fixed at 0.01 M (0.48% Mg/feedstock mass ratio). For comparison, unmodified WRB was also produced at the same designated temperatures.

2.3 Biochar characterization

After obtaining the biochars under different conditions, they were thoroughly characterized. The details of the characterization are presented in the supporting information (SI). Briefly, the biochar pH was measured in aqueous solution with a pH meter; the BET surface area was measured by N_2 adsorption/desorption; the Mg content was determined by acid digestion and inductively coupled plasma optical emission spectrometry (ICP-OES); the molecular structure was tested by Fourier transform infrared spectroscopy (FTIR); and, the mineral composition was analyzed by X-ray diffraction (XRD).

2.4 Lead removal test

Removal tests were carried out in order to understand the ability of the MWRBs to remove Pb. Pb was selected as a representative heavy metal contaminant, because unmodified WRB revealed a higher adsorption capacity for Pb among different heavy metals and there is an urgent need to remediate lead in soil and water as mentioned. For each removal test, 0.1 g of biochar was added to 20 mL of 50 mM $Pb(NO_3)_2$ solution. The mixture was shaken at 250 rpm for 24h to reach adsorption equilibrium. The aqueous solution was separated from the solids by centrifugation at 4000 rpm for 4 min and filtration (0.22 μm), and analyzed for Pb concentration by ICP-OES.

2.5 Quality assurance and statistical analysis

Experiments were conducted in duplicate, apart from XRD and FT-IR tests owing to cost and time restrictions. Mean and standard deviation data are presented for duplicated experiments.

3 Results and discussion

3.1 Effect of excessive impregnation on Mg content of biochar

The unmodified WRB had an Mg content of 0.62%, and the Mg content of the MWRBs increased from 1.52% to 10.1% by increasing the initial Mg/feedstock ratios (Figure 1).

Although the observed increasing trend in Mg content was not linear, tailing off at higher Mg/feedstock ratios, it can be seen that the Mg content coated on MWRB is directly proportional to the initial Mg/feedstock mass ratio, and so it can be controlled accordingly. A simple logarithmic relationship (Equation 1) with R^2 of 0.982 can be obtained between Mg content of MWRB and initial Mg/feedstock mass ratio, which can be referred for future studies.

$$y=3.51\ln(x+1.28) \quad \text{Equation 1}$$

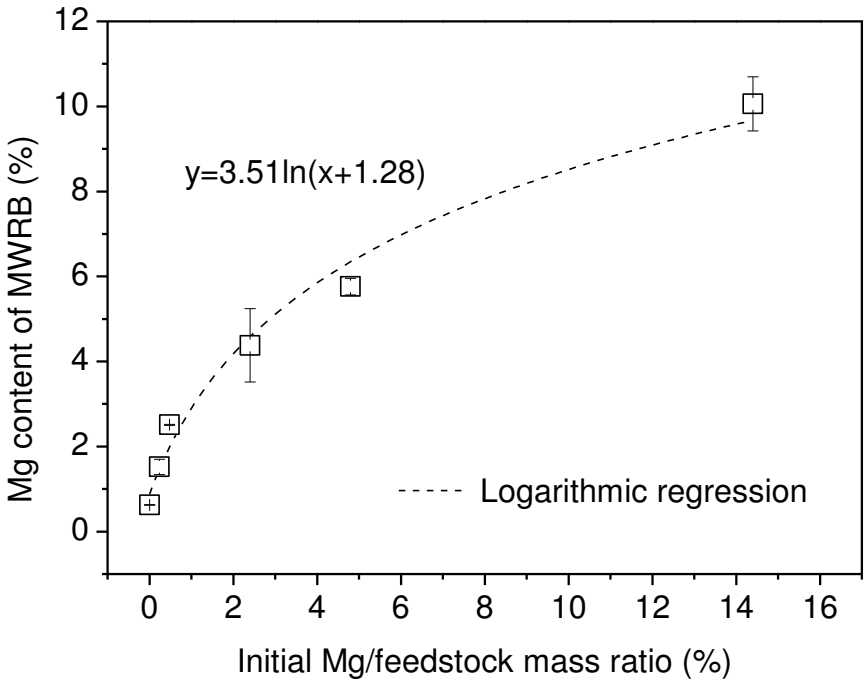

Figure 1 Mg content of MgO-coated watermelon rind biochars (MWRBs) synthesized using excessive impregnation pretreatment at different initial Mg/feedstock mass ratios (0 represents raw watermelon rind biochar (WRB))

3.2 Effect of Mg content on biochar characteristics

The effect of Mg content on the BET surface area and Pb removal capacity of the MWRBs is shown in Figure 2. Regarding the BET surface area, the unmodified WRB had a low surface area of 1 m^2/g, suggesting a poor porous structure. The modification significantly enhanced the surface area of MWRB, climbing to a

maximum of 293 m^2/g for the MWRB with 2.51% Mg coating. It dropped to 150 m^2/g when Mg content of MWRB increased to 4.38%, and then gradually decreased to 86.1 m^2/g at 10.1% Mg. Therefore, an optimal Mg content for the highest BET surface of MWRB was observed within the investigated range

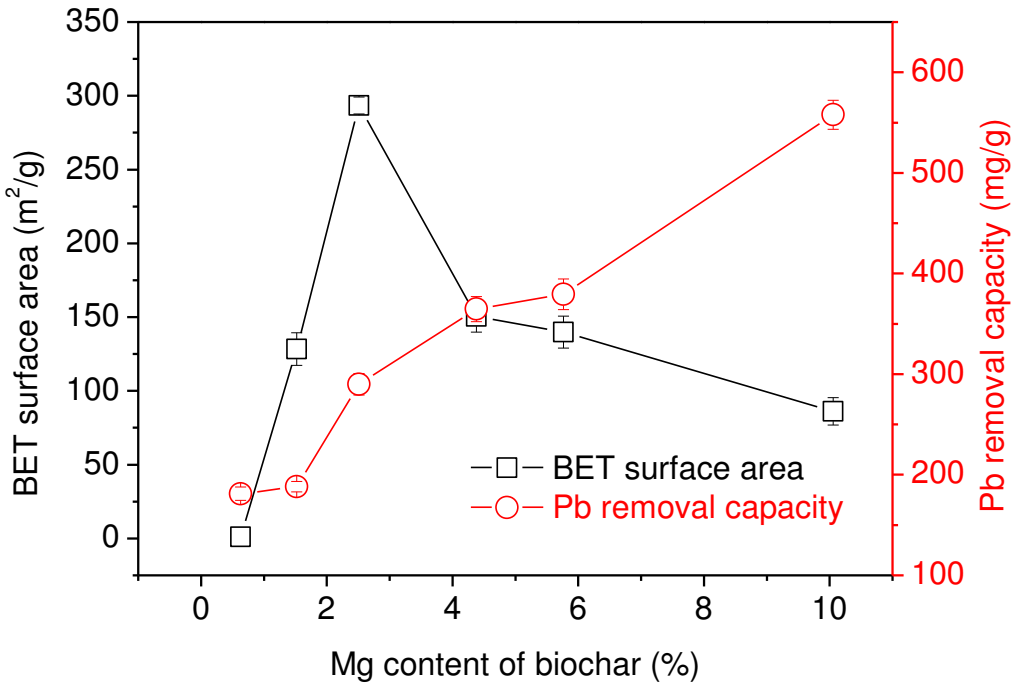

Figure 2 Effects of Mg content on the BET surface area and Pb removal capacity of MgO-coated watermelon rind biochars (MWRBs)

The $MgCl_2$ pretreatment activated the resultant biochar pore structure because it can strongly dehydrate carbohydrate polymers (Li et al., 2016), resulting in the accelerated release of volatile matter and the formation of open pores under heating (Shen et al., 2019b). However, with greater $MgCl_2$ concentrations, the thermal decomposition of hydrated $MgCl_2$ results in the formation of excess MgO and other intermediate products (Huang et al., 2011) that block pores, leading to decreased biochar surface area. Li et al. (2016) investigated the surface area of magnesium magnetic sugarcane harvest residue biochar, and they observed an optimal BET surface area at an Mg content of 2.12% over an Mg content range of 0.43-20.47% (Li

et al., 2016). Their finding corroborates the finding of present study, with a similar optimal biochar Mg content. The pH values of all MWRBs was in the range of 10.49-10.72 (Figure S1), which was similar to the unmodified WRB (10.98), suggesting the modification did not significantly alter the pH of biochar.

The XRD patterns of WRB and MWRBs are shown in Figure 3. The unmodified WRB revealed the presence of KCl and aphthitalite ($(K,Na)_3Na(SO_4)_2$). Potassium (K) and sodium (Na) are abundant elements in watermelon rind (Egbuonu, 2015). Therefore, the formation of minerals containing K and Na after pyrolysis could be expected (Li et al., 2019; Shen et al., 2017a; Shen et al., 2017b). After modification, characteristic peaks of MgO (Jin and Al-Tabbaa, 2014a) occurred on the XRD patterns, with their strength significantly increasing with increased Mg content, suggesting successful coating of MgO, and the MgO content being directly related to the Mg content. As the MWRB Mg content increased to 10.1%, two new peaks representing $Mg(OH)_2$ occurred on the XRD pattern. This may be due to the greater energy demand for thermal decomposition of hydrated $MgCl_2$, and, therefore, a certain amount of $Mg(OH)_2$ was formed as an intermediate product (Huang et al., 2011). This assumption is supported by the previous finding that $Mg(OH)_2$ formed during the thermal decomposition of hydrated $MgCl_2$ and corncob mixture at a Mg content of 17.9% (Shen et al., 2019b). Due to the introduction of chlorine (Cl) with Mg, the strength of the peaks representing KCl also increased with increasing Mg content. However, at Mg contents higher than 5.76%, their strength decreased because the formed MgO will have diluted the KCl concentrations, and it may also have coated over the KCl surfaces. These may also explain the decrease in the peak intensity representing $(K,Na)_3Na(SO_4)_2$.

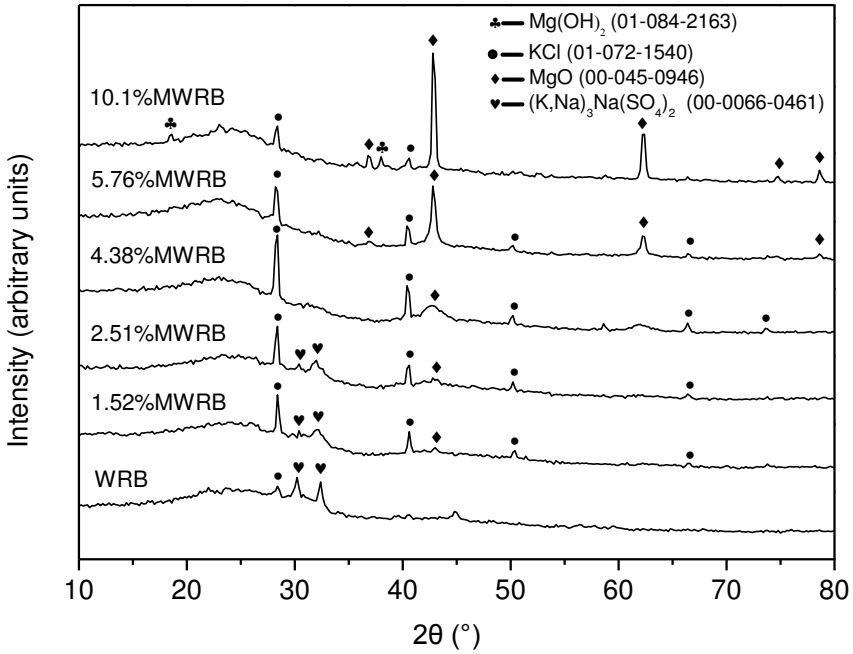

Figure 3 XRD patterns of watermelon rind biochar (WRB) and MgO-coated watermelon rind biochars (MWRBs) with different Mg content (the numbers in brackets represent PDF card numbers)

The FTIR spectra of WRB and MWRBs with different Mg contents are shown in Figure 4. Two peaks were observed for WRB. The peaks at 1570 cm^{-1} represent aromatic C=C, which were typically observed for plant-based biochar (Wang et al., 2017; Zhang et al., 2017a). The peaks at 1060 cm^{-1} are attributed to aliphatic C-O-C originated from the raw watermelon rind (Jawad et al., 2018), which are also typical FTIR peaks for biochar (Shen et al., 2018d). After modification, the aromatic C=C peak (1060 cm^{-1}) significantly strengthened as the Mg content of biochar increased to 2.51%. Similarly, the peaks representing substituted aromatic C-H (1040 cm^{-1}) (Keiluweit et al., 2010) was greatly enhanced after modification. Three new peaks representing aromatic C-H (870, 810, and 750 cm^{-1}) occurred on the FTIR spectra of MWRBs. These suggest that the aromaticity of biochar was significantly enhanced after modification. As mentioned, the presence of $MgCl_2$ activates biochar during heating, facilitating the volatilization of organic materials. The increased volatilization

resulted in the increased aromatic structure of biochar. It was observed that 2.51% Mg was the optimal content for a maximum surface area of MWRB (Figure 2). The FTIR results further confirm this, because all the peaks (1060, 1040, 870, 810, and 750 cm^{-1}) related to aromatic C on FTIR spectra reached their highest strength for the MWRB with 2.51% Mg content. These peaks decreased for MWRB with further Mg content, suggesting that the activation efficiency decreased. Another plausible reason may be the MgO on the biochar surface affecting the detection of aromatic C by the FTIR test. Carboxylic and phenolic groups were not observed, because they have already decomposed at such high pyrolysis temperature (Keiluweit et al., 2010).

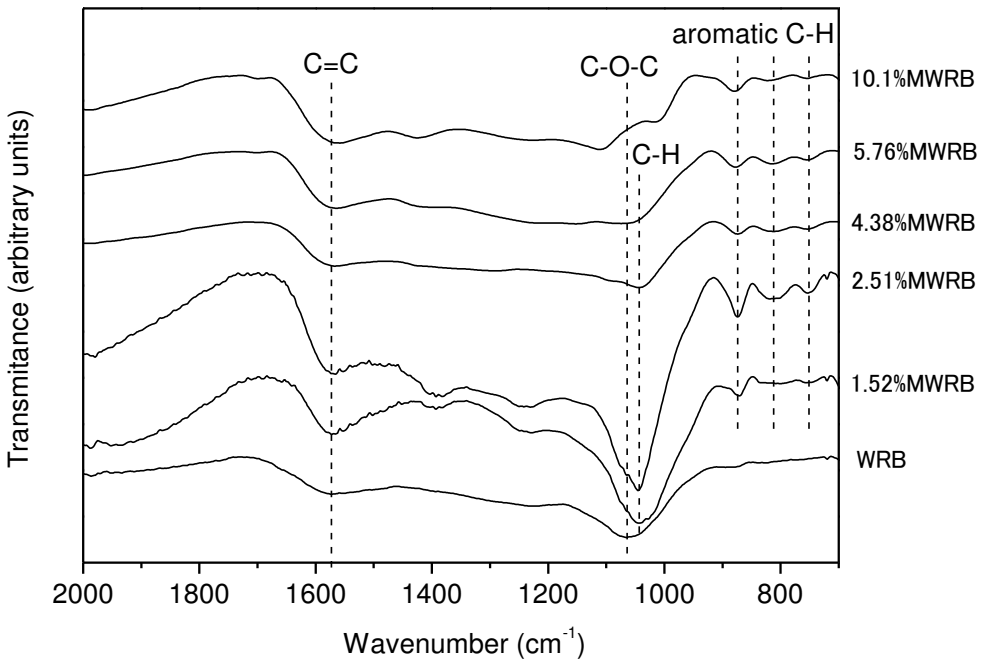

Figure 4 FTIR spectra of watermelon rind biochar (WRB) and MgO-coated watermelon rind biochars (MWRBs) with different Mg content

3.3 Effect of pyrolysis temperature on biochar characteristics

The effects of pyrolysis temperature on the BET surface area and Mg content of MWRBs are shown in Figure 5. The surface area of MWRB drastically increased as the maximum pyrolysis temperature was increased from 400 to 600°C, peaking at

600°C (293 m^2/g). It slightly decreased to 250 m^2/g at 700°C and then dropped to 59.8 m^2/g at the final pyrolysis temperature of 800°C. Optimal pyrolysis temperatures for maximum surface area have also been observed in the range of 500-900°C in previous studies (Antal et al., 2003). At relatively low temperatures (< 600°C), an increase of pyrolysis temperature facilitates the volatilization of organics and therefore increases the porosity of the formed biochar (Zhao et al., 2018). However, at higher temperatures, further increases in temperature can result in blocked pores due to greater ash formation, and micropores shrink leading to a reduction in the open porosity (Antal et al., 2003).

It is of note that the unmodified WRB had a BET surface area of only 1 m^2/g, therefore, it can be inferred that the $MgCl_2$ greatly contributed to the volatilization of the organics in watermelon rind, aiding the development of biochar porosity. The Mg content of the MWRBs produced at different temperatures were in the range of 1.89-2.51%, as the original Mg/feedstock ratio for the MWRBs produced at different temperatures was fixed at 0.48%. This suggests that the biochar yield at the temperature range of 400-800°C did not vary significantly, which is in line with previous findings that the yield of rice straw biochars produce in the range of 500-700°C (Shen et al., 2019a).

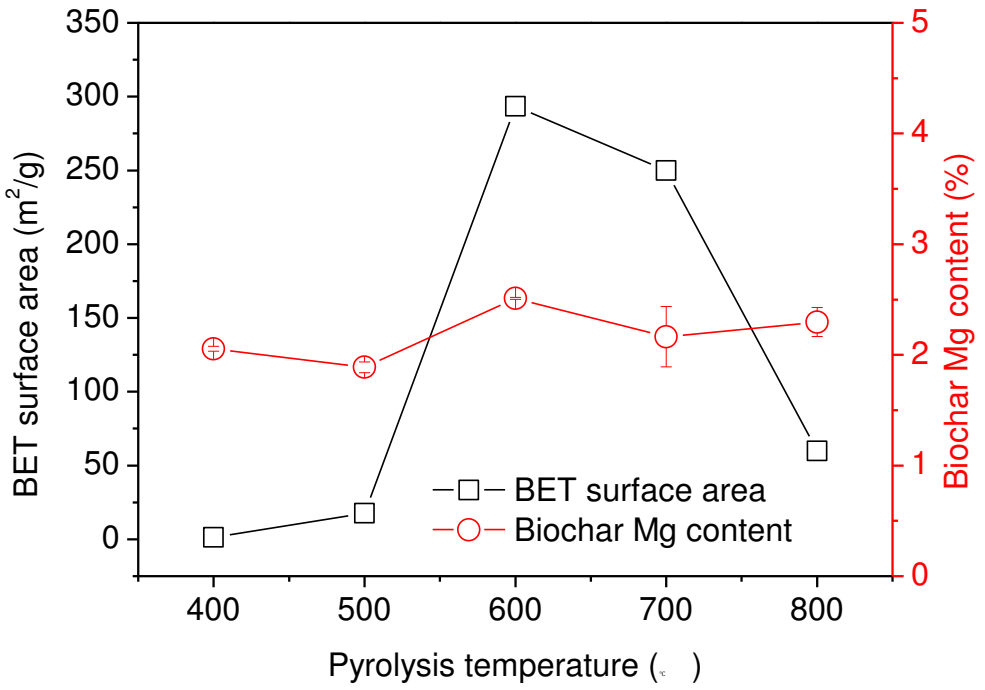

Figure 5 Effects of pyrolysis temperature on the BET surface area and Mg content of MgO-coated watermelon rind biochars (MWRBs) (Mg/feedstock mass ratio of 0.48%)

The XRD patterns of the MWRBs produced at different temperatures are shown in Figure 6. The MgO peaks for MWRBs produced at 500-800°C were similar, suggesting similar MgO contents. However, MgO peaks were not observed for MWRB produced at 400°C, because the thermal decomposition of hydrated $MgCl_2$ to MgO happens at temperatures greater than 360-412°C (Huang et al., 2011). For the MWRBs produced at 500-800°C, the thermal decomposition of hydrated $MgCl_2$ was complete, therefore, the produced MgO content was similar.

The KCl peak in MWRBs produced at 500-700°C was similar, however its strength was significantly weaker for those produced at 400°C and 800°C. At 400 °C, the K was generally in the form of carboxylates, with relatively small amounts of KCl formed (Dodson, 2011). At 800 °C, the Cl may have volatilized in the form of HCl, and K may exist in the form of K_2O, which may not be detected by XRD tests due to the relatively low concentration (Dodson, 2011; Shen et al., 2019b).

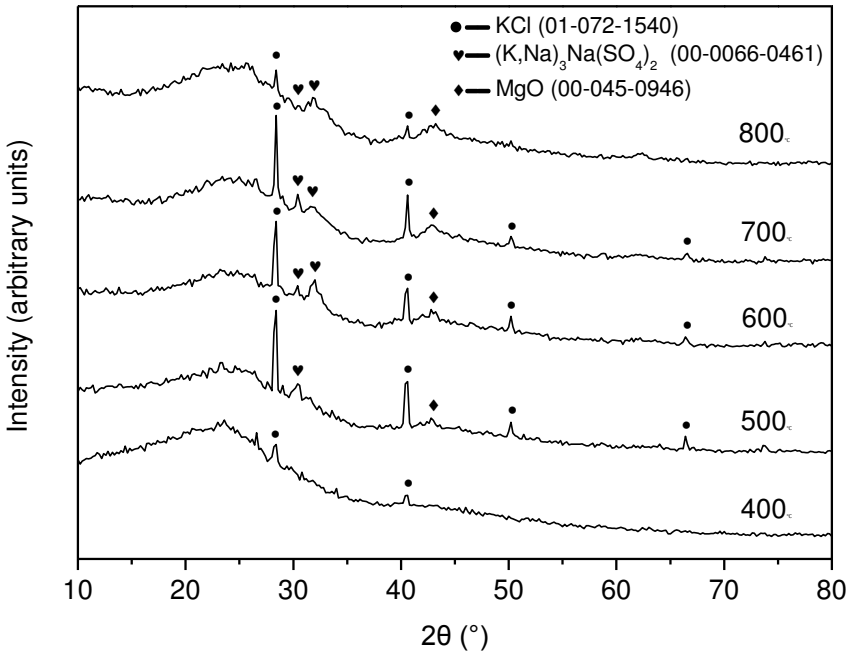

Figure 6 XRD patterns of MgO-coated watermelon rind biochars (MWRBs) produced at different temperatures (Mg/feedstock mass ratio of 0.48%) (the numbers in brackets represent PDF card numbers)

The FTIR of the MWRBs produced at different temperatures are shown in Figure 7. It can be observed that pyrolysis temperature greatly affected the functionality of the biochars. The peaks representing aromatic C (1060, 1040, 870, 810, and 750 cm^{-1}) increased as pyrolysis temperature increased from 400 to 600°C and then diminished from 600 to 800°C. The increased dehydration and volatilization of cellulose, hemicellulose, and lignin at 400-600°C resulted in the development of aromatic C (Keiluweit et al., 2010). At > 600°C, the condensation of the aromatic units to larger sheets reduces these aromatic peaks (Keiluweit et al., 2010). The peaks representing aliphatic CH_2 and aliphatic C-O-C decreased, with increased decomposition of aliphatic structures as the maximum pyrolysis temperature was increased.

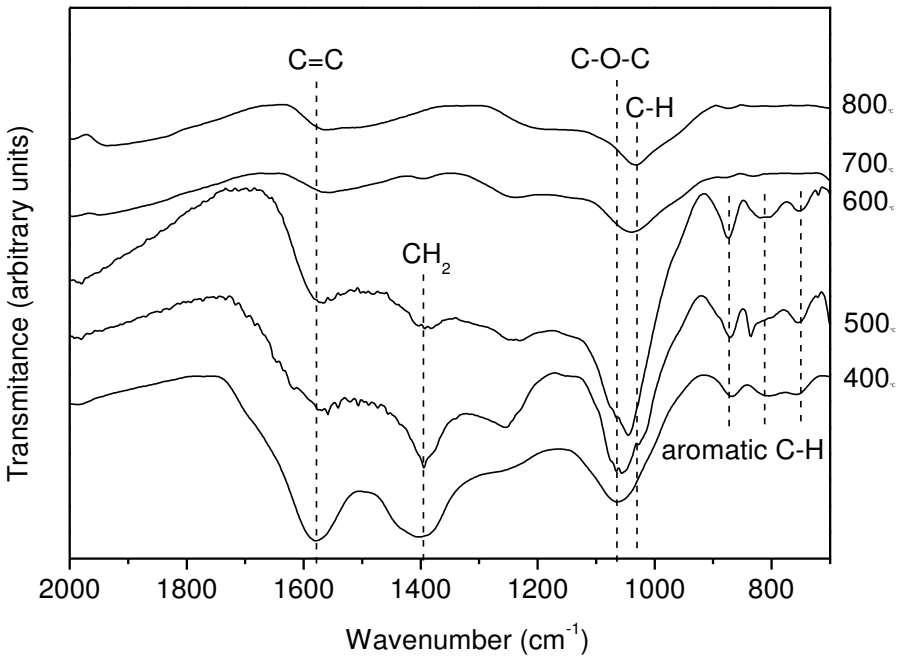

Figure 7 FT-IR spectra of MgO-coated watermelon rind biochars (MWRBs) produced at different temperatures (Mg/feedstock mass ratio of 0.48%)

3.4 Lead removal

The effect of Mg content on the Pb removal capacity of MWRBs was shown in Figure 2. The modification significantly enhanced the Pb removal capacity of MWRB, and the efficiency increased with increasing Mg content. The highest Pb removal capacity (558 mg/g) was found at the highest Mg content (10.1% Mg), an increase of 208% over the 181 mg/g of the unmodified WRB. Two factors are attributed to the increased Pb removal capacity of MWRB. One is the increased surface area of biochar; it is well established that higher surface area of biochar can aid the adsorption/removal of heavy metals due to enhanced contact between metals and biochar (Shen et al., 2015; Shen et al., 2017b). The other is the effect of the MgO coating. Although the pH value of MWRB was not significantly changed compared to WRB (Figure S1), the buffering capacity was enhanced considerably (Shen et al., 2018c; Wang et al., 2018b).

Therefore, greater amounts of Pb can be precipitated after modification. In addition to precipitation, MgO and its hydration products $Mg(OH)_2$ can also aid the removal of Pb through physical sorption, cation exchange, and complexation (Jin and Al-Tabbaa, 2014b; Jin et al., 2016). The increased Pb removal capacity for MWRBs with the highest Mg contents suggests that the increased buffering capacity, rather than surface area, was the main contributor to Pb removal. If surface area had been the main factor, the Pb removal capacity would have decreased as Mg content of the MWRB was increased from 2.51% to 10.1% with decreased surface areas. Therefore, MgO was the main contributor to increased Pb removal. It is of note that the greatest increase in Pb removal (as a percentage of Mg added) was observed in the Mg range 1.52-2.51% (Figure 2). This may be due to the strong increase of biochar surface area, and the increased formation of MgO in biochar at this Mg content range.

The effect of pyrolysis temperature on the Pb removal capacity of WRB and MWRB is shown in Figure 8. The Pb removal capacity of the unmodified WRB increased with increasing pyrolysis temperature owing to the formation of alkaline minerals (e.g. K_2O) and greater aromaticity, aiding precipitation and cation-π adsorption of Pb (Dodson, 2011; Shen et al., 2019b).

The Pb removal capacity of MWRB increased from 81.7 mg/g (at 400°C) to 742 mg/g (at 700°C), and then dropped to 368 mg/g (at 800°C). The Pb removal capacity of the MWRB was generally much higher than WRB due to increased surface area and MgO coating. However, for the MWRBs produced at 400°C and 800 °C, the Pb removal capacity was lower than the respective WRB counterparts. As discussed above, MgO was not observed for MWRB produced at 400°C; on the contrary, other Mg- minerals formed may have blocked the pores of the biochar, thus inhibiting the adsorption/removal of Pb. At 800 °C, although considerable amounts of MgO formed, the reactivity of the formed MgO was lower than that formed at lower temperatures (Garcia et al., 2004; Jin and Al-Tabbaa, 2014a), which may have reduced its ability to remove Pb. In addition, the large amount of (low-reactive) MgO and other Mg-

minerals may encapsulate the alkaline minerals in the biochar, which inhibited their hydration and the precipitation of Pb. In general, the Pb removal capacities of the MWRBs are outstanding compared with other modified biochars and biochar composites (Table 1).

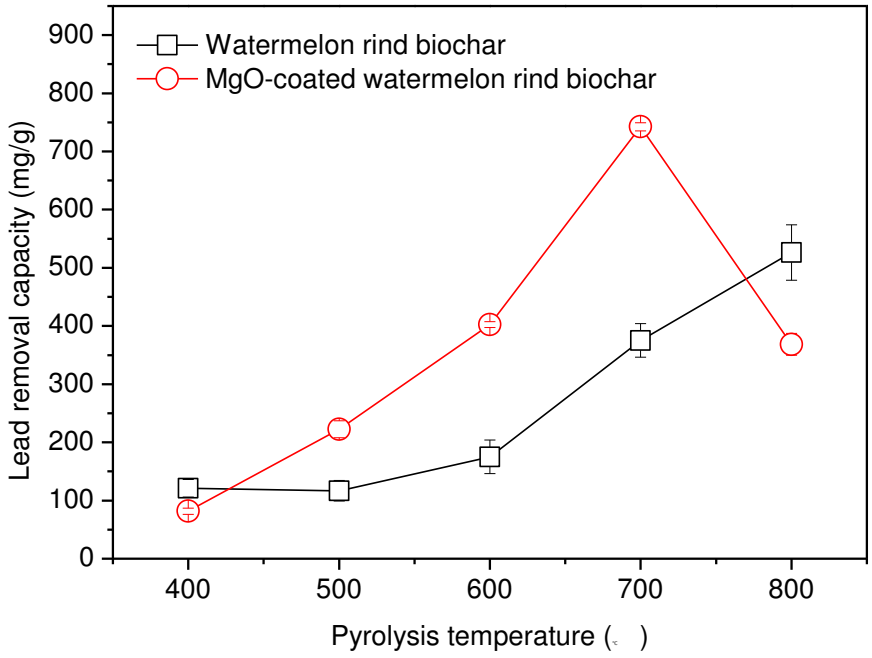

Figure 8 Lead removal capacity of watermelon rind biochar and MgO-coated water melon rind biochar (Mg content of 2.51%)

Table 1 Lead removal/adsorption capacity (mg/g) of biochar composite or modified biochar from existing literature and in the present work

Composite or modified biochar	Pyrolysis temperature (°C)	Maximum adsorption/removal capacity (mg/g)	References
Watermelon rind biochar	600	181	The present work
Watermelon rind biochar	700	375	
MgO-coated watermelon rind biochar	600	558	
MgO-coated watermelon rind biochar	700	742	
Corncob biochar/montmorillonite composite	400	153	(Fu et al., 2020)
H_3PO_4 pretreated miscanthus sacchariflorus hydrothermal biochar	200	316	(Zhou et al., 2019)
Fe-Mn-S/corn straw hydrothermal biochar composite	120	182	(Yang et al., 2019)
HCl pretreated date seed biochar	550	189	(Mahdi et al., 2019)
Iron activated reed biochar	450	17.5	(Cui et al., 2019)
H_3PO_4 pretreated chicken feather biochar	450	78.4	(Chen et al., 2019a)
Urea-functionalized magnetic palm biochar	400	188	(Zhou et al., 2018)
Biochar-supported reduced graphene oxide composite	600	34.0	(Zhang et al., 2018b)
Eggshell pretreated biochars	450	103-261	(Wang et al., 2018a)

Biochar-supported hydrated manganese oxide nanoparticles	400	110	(Wan et al., 2018)
Magnetized Douglas fir biochar	900-1000	27	(Karunanayake et al., 2018)
Chitosan modified biochar	425	134	(Dewage et al., 2018)
Microwave heated magnetic coconut shell biochar	Not available	4.10	(Yap et al., 2017)
H_2O_2 modified coconut fiber-derived biochar	700	92.4	(Wu et al., 2017)
$NH_3 \cdot H_2O$ modified coconut fiber-derived biochar	300	106	
HNO_3 modified coconut fiber-derived biochar	300	85.2	
NaOH modified dairy manure biochar	300	192	(Yuan et al., 2016)
$MgCl_2$ pretreated sawdust biochar	600	202	(Jellali et al., 2016)
NaOH modified hickory wood biochar	600	53.6	(Ding et al., 2016)
Manganese-oxide/biochar composite	700	93.4	(Wang et al., 2015a)

3.5 Environmental implications

In order to optimize performance in environmental applications, such as soil remediation, water treatment, and catalysis, biochar selection is often based on BET surface area. In this study, a maximum surface area of 293 m^2/g was achieved for MWRB by increasing the Mg content to 2.51%, and using an optimal pyrolysis temperature of 600°C.

The unmodified WRB produced at 600°C had a Pb removal capacity of 181 mg/g, which is relatively high in comparison to biochars produced from other feedstocks (Gao et al., 2019). Furthermore, the modification greatly enhanced the MWRB Pb removal capacity to 558 mg/g (at 600°C), at an Mg content of 10.1%. Although further increases of Mg content may result in a higher Pb removal capacity, the modification cost will also increase. In industrial manufacturing, higher Mg content and synthesis temperature can lead to higher costs. Therefore, a balance between the cost and performance for MWRB production should be found out, depending on the remediation scenario. It should also be noted that $MgCl_2$ is abundant in natural resources (sea water) and industrial wastes (brine water) (Ye et al., 2018). The sustainable utilization of $MgCl_2$ from these sources can partly lower the costs and life-cycle carbon footprint.

The MWRB produced at 700°C (at Mg/feedstock of 0.48%) displayed the highest Pb removal capacity (742 mg/g), although the surface area achieved (250 m^2/g) was not the greatest. Therefore, from the point of view of Pb removal, greater attention should be paid to biochar's buffering capacity. Further studies are required to investigate the optimal temperature for Pb removal at different Mg/feedstock ratios, balancing the cost and performance.

4 Conclusions

In this study, the effects of excessive impregnation, pyrolysis temperature, and Mg content, on synthesized MWRB were investigated. The Mg content of MWRBs can be

controlled by adjusting the initial Mg/feedstock mass ratio, following a logarithmic relationship. The modification significantly enhanced the surface area of the MWRB, with the BET surface area increasing first and then decreasing as the Mg content of biochar increased from 0.63% to 10.1%, with an optimal value 293 m^2/g found for MWBR with an Mg content of 2.51%, whereas the surface area of the unmodified WRB was only 1 m^2/g. The increased Mg content of the MWRBs aided the formation of MgO, and FTIR peaks representing aromatic C was also increased, being at their maximum in the MWRB with an Mg content of 2.51%.

For a fixed Mg/feedstock ratio of 0.48% (resulting in MWRBs with Mg contents of 1.89-2.51%), the BET surface area of MWRB also increased as the pyrolysis temperature was increased from 400°C to 600°C, and then decreased with increasing temperature from 600 to 800°C, with an optimal value of 293 m^2/g found at 600°C. Increased pyrolysis temperature also aided the formation of MgO, but the reactivity of the MgO formed may be reduced at the highest pyrolysis temperatures. The peaks representing aromatic C of MWRBs peaked at 600°C.

The effects of Mg content and pyrolysis temperature on the Pb removal capacity of MWRBs was also investigated. The Pb removal capacity of MWRB (produced at 600°C) increased with increasing Mg content (0.63-10.1%), with the highest Pb removal capacity of 558 mg/g achieved at the highest Mg content (10.1%), an improvement of 208% over that of unmodified WRB (181 m^2/g). It is notable that the highest Pb removal capacity achieved did not coincide with the highest surface area but rather the highest Mg content. After pre-treatment using an Mg/feedstock ratio of 0.48%, the Pb removal capacity of the MWRB could be increased by increasing the pyrolysis temperature; from 81.7 mg/g when pyrolyzed at 400°C, to 742 mg/g at 700°C, but dropping to 368 mg/g at 800°C.

Acknowledgements

This work was supported by China's National Water Pollution Control and Treatment Science and Technology Major Project (Grant No. 2018ZX07109-003), and the

National Key Research and Development Program of China (Grant No. 2018YFC1801300). The third author would like to thank the Killam Trusts of Canada for kindly providing the Izaak Walton Killam Memorial Postdoctoral Fellowship.

References

Ahmad, M., et al., 2014. Biochar as a sorbent for contaminant management in soil and water: A review. Chemosphere. 99, 19-33.

Antal, M. J., et al., 2003. The art, science, and technology of charcoal production. 42, 1619-1640.

Cao, L. C., et al., 2018. Phosphoric acid-activated wood biochar for catalytic conversion of starch-rich food waste into glucose and 5-hydroxymethylfurfural. Bioresource Technology. 267, 242-248.

Chen, H. Y., et al., 2019a. Adsorption of cadmium and lead ions by phosphoric acid-modified biochar generated from chicken feather: Selective adsorption and influence of dissolved organic matter. Bioresource Technology. 292.

Chen, L., et al., 2019b. Sustainable stabilization/solidification of municipal solid waste incinerator fly ash by incorporation of green materials. Journal of Cleaner Production.

Cui, L. Q., et al., 2019. Mechanism of Adsorption of Cadmium and Lead Ions by Iron-activated Biochar. Bioresources. 14, 842-857.

Dewage, N. B., et al., 2018. Lead (Pb2+) sorptive removal using chitosan-modified biochar: batch and fixed-bed studies. Rsc Advances. 8, 25368-25377.

Ding, Z. H., et al., 2016. Removal of lead, copper, cadmium, zinc, and nickel from aqueous solutions by alkali-modified biochar: Batch and column tests. Journal of Industrial and Engineering Chemistry. 33, 239-245.

Dodson, J., Wheat straw ash and its use as a silica source. University of York, 2011.

Egbuonu, A. C. C. J. A. J. o. B., 2015. Comparative assessment of some mineral, amino acid and vitamin compositions of watermelon (Citrullus lanatus) rind and seed. 10, 230-236.

Fu, C. L., et al., 2020. The single/co-adsorption characteristics and microscopic adsorption mechanism of biochar-montmorillonite composite adsorbent for pharmaceutical emerging organic contaminant atenolol and lead ions. Ecotoxicology and Environmental Safety. 187.

Gao, R., et al., 2019. Highly-effective removal of Pb by co-pyrolysis biochar derived from rape straw and orthophosphate.

Garcia, M. A., et al., 2004. Low-grade MgO used to stabilize heavy metals in highly contaminated soils. Chemosphere. 56, 481-91.

Hou, D., et al., 2018. A Sustainability Assessment Framework for Agricultural Land Remediation in China. Land Degradation & Development. 29, 1005-1018.

Huang, Q. Z., et al., 2011. Thermal decomposition mechanisms of MgCl2 center dot 6H(2)O and MgCl2 center dot H2O. Journal of Analytical and Applied Pyrolysis.

91, 159-164.
Inyang, M. I., et al., 2016. A review of biochar as a low-cost adsorbent for aqueous heavy metal removal. Critical Reviews in Environmental Science & Technology. 46, 00-00.
Jawad, A. H., et al., 2018. Utilization of watermelon (Citrullus lanatus) rinds as a natural low-cost biosorbent for adsorption of methylene blue: kinetic, equilibrium and thermodynamic studies. 12, 371-381.
Jellali, S., et al., 2016. Lead removal from aqueous solutions by raw sawdust and magnesium pretreated biochar: Experimental investigations and numerical modelling. Journal of Environmental Management. 180, 439-449.
Jin, F., Al-Tabbaa, A., 2014a. Characterisation of different commercial reactive magnesia. Advances in Cement Research. 26, 101-113.
Jin, F., Al-Tabbaa, A., 2014b. Evaluation of novel reactive MgO activated slag binder for the immobilisation of lead and zinc. Chemosphere. 117, 285-94.
Jin, F., et al., 2016. Three-year performance of in-situ solidified/stabilised soil using novel MgO-bearing binders. Chemosphere. 144, 681-8.
Jung, K. W., Ahn, K. H., 2016. Fabrication of porosity-enhanced MgO/biochar for removal of phosphate from aqueous solution: Application of a novel combined electrochemical modification method. Bioresour Technol. 200, 1029-32.
Kang, X., et al., 2019. Hydration of C3A/gypsum composites in the presence of graphene oxide. 100889.
Karunanayake, A. G., et al., 2018. Lead and cadmium remediation using magnetized and nonmagnetized biochar from Douglas fir. Chemical Engineering Journal. 331, 480-491.
Keiluweit, M., et al., 2010. Dynamic Molecular Structure of Plant Biomass-Derived Black Carbon (Biochar). Environmental Science & Technology. 44, 1247-1253.
Lam, S. S., et al., 2016. Fruit waste as feedstock for recovery by pyrolysis technique. International Biodeterioration & Biodegradation. 113, 325-333.
Li, H., et al., 2019. Biochar derived from watermelon rinds as regenerable adsorbent for efficient removal of thallium (I) from wastewater. 127, 257-266.
Li, R., et al., 2016. Recovery of phosphate from aqueous solution by magnesium oxide decorated magnetic biochar and its potential as phosphate-based fertilizer substitute. Bioresour Technol. 215, 209-214.
Ling, L. L., et al., 2017. Magnesium Oxide Embedded Nitrogen Self-Doped Biochar Composites: Fast and High-Efficiency Adsorption of Heavy Metals in an Aqueous Solution. Environ Sci Technol. 51, 10081-10089.
Mahdi, Z., et al., 2019. Preparation, characterization and application of surface modified biochar from date seed for improved lead, copper, and nickel removal from aqueous solutions. Journal of Environmental Chemical Engineering. 7.
Mohanty, S. K., et al., 2018. Plenty of room for carbon on the ground: Potential applications of biochar for stormwater treatment. Science of the Total Environment. 625, 1644-1658.
O'Connor, D., et al., 2018a. Lead-based paint remains a major public health concern:

A critical review of global production, trade, use, exposure, health risk, and implications. Environment international. 121, 85-101.

O'Connor, D., et al., 2018b. Sulfur-modified rice husk biochar: A green method for the remediation of mercury contaminated soil. Science of the Total Environment. 621, 819-826.

O'Connor, D., et al., 2018c. Biochar application for the remediation of heavy metal polluted land: A review of in situ field trials. Sci Total Environ. 619-620, 815-826.

Rajapaksha, A. U., et al., 2016. Engineered/designer biochar for contaminant removal/immobilization from soil and water: Potential and implication of biochar modification. Chemosphere. 148, 276-291.

Shen, Z., et al., 2018a. Assessing long-term stability of cadmium and lead in a soil washing residue amended with MgO-based binders using quantitative accelerated ageing. Science of The Total Environment. 643, 1571-1578.

Shen, Z., et al., 2018b. Lead-based paint in children's toys sold on China's major online shopping platforms. Environ Pollut. 241, 311-318.

Shen, Z., et al., 2018c. Stability of heavy metals in soil washing residue with and without biochar addition under accelerated ageing. Sci Total Environ. 619-620, 185-193.

Shen, Z., et al., 2015. Sorption of lead by Salisbury biochar produced from British broadleaf hardwood. Bioresour Technol. 193, 553-6.

Shen, Z., et al., 2018d. Mechanisms of biochar assisted immobilization of Pb(2+) by bioapatite in aqueous solution. Chemosphere. 190, 260-266.

Shen, Z., et al., 2017a. Qualitative and quantitative characterisation of adsorption mechanisms of lead on four biochars. 609, 1401-1410.

Shen, Z., et al., 2017b. Characteristics and mechanisms of nickel adsorption on biochars produced from wheat straw pellets and rice husk. 24, 12809-12819.

Shen, Z. T., et al., 2019a. Effect of production temperature on lead removal mechanisms by rice straw biochars. Science of the Total Environment. 655, 751-758.

Shen, Z. T., et al., 2016. Salisbury biochar did not affect the mobility or speciation of lead in kaolin in a short-term laboratory study. Journal of Hazardous Materials. 316, 214-220.

Shen, Z. T., et al., 2019b. Synthesis of MgO-coated corncob biochar and its application in lead stabilization in a soil washing residue. Environment International. 122, 357-362.

Shi, T., et al., 2019. Status of lead accumulation in agricultural soils across China (1979–2016). 129, 35-41.

Song, Y., et al., 2019. Nature based solutions for contaminated land remediation and brownfield redevelopment in cities: A review. Science of the Total Environment. 663, 568-579.

Suliman, W., et al., 2016. Modification of biochar surface by air oxidation: Role of pyrolysis temperature. Biomass and Bioenergy. 85, 1-11.

Tang, J. C., et al., 2013. Characteristics of biochar and its application in remediation of contaminated soil. Journal of Bioscience and Bioengineering. 116, 653-659.

Wan, S. L., et al., 2018. Enhanced lead and cadmium removal using biochar-supported hydrated manganese oxide (HMO) nanoparticles: Behavior and mechanism. Science of the Total Environment. 616, 1298-1306.

Wang, H., et al., 2017. Sorption of tetracycline on biochar derived from rice straw under different temperatures. PLoS One. 12, e0182776.

Wang, H. Y., et al., 2018a. Engineered biochar derived from eggshell-treated biomass for removal of aqueous lead. Ecological Engineering. 121, 124-129.

Wang, L., et al., 2019a. Novel synergy of Si-rich minerals and reactive MgO for stabilisation/solidification of contaminated sediment. Journal of hazardous materials. 365, 695-706.

Wang, L., et al., 2019b. Green remediation of As and Pb contaminated soil using cement-free clay-based stabilization/solidification. Environment international. 126, 336-345.

Wang, L., et al., 2018b. Low-carbon and low-alkalinity stabilization/solidification of high-Pb contaminated soil. Chemical Engineering Journal. 351, 418-427.

Wang, M. C., et al., 2015a. A novel manganese-oxide/biochar composite for efficient removal of lead(II) from aqueous solutions. International Journal of Environmental Science and Technology. 12, 1719-1726.

Wang, S., et al., 2015b. Manganese oxide-modified biochars: preparation, characterization, and sorption of arsenate and lead. Bioresour Technol. 181, 13-7.

Wang, S., et al., 2015c. Manganese oxide-modified biochars: Preparation, characterization, and sorption of arsenate and lead. Bioresour Technol. 181, 13-17.

Wang, Y., et al., 2019c. One-pot green synthesis of bimetallic hollow palladium-platinum nanotubes for enhanced catalytic reduction of p-nitrophenol. Journal of Colloid and Interface Science. 539, 161-167.

Wu, W. D., et al., 2017. Unraveling sorption of lead in aqueous solutions by chemically modified biochar derived from coconut fiber: A microscopic and spectroscopic investigation. Science of the Total Environment. 576, 766-774.

Xiao, R., et al., 2018. Enhanced sorption of hexavalent chromium [Cr (VI)] from aqueous solutions by diluted sulfuric acid-assisted MgO-coated biochar composite. 208, 408-416.

Yang, F., et al., 2019. Porous biochar composite assembled with ternary needle-like iron-manganese-sulphur hybrids for high-efficiency lead removal. Bioresource Technology. 272, 415-420.

Yang, X., et al., 2018. Characterization of bioenergy biochar and its utilization for metal/metalloid immobilization in contaminated soil. Science of the Total Environment. 640, 704-713.

Yao, Y., et al., 2013. Engineered carbon (biochar) prepared by direct pyrolysis of Mg-accumulated tomato tissues: Characterization and phosphate removal

potential. Bioresource Technology. 138, 8-13.
Yap, M. W., et al., 2017. Microwave induced synthesis of magnetic biochar from agricultural biomass for removal of lead and cadmium from wastewater. Journal of Industrial and Engineering Chemistry. 45, 287-295.
Ye, Z. L., et al., 2018. Fractionating magnesium ion from seawater for struvite recovery using electrodialysis with monovalent selective membranes. Chemosphere. 210, 867-876.
Yuan, Z. H., et al., Dairy manure biochar modified with sodium hydroxide and its effect on lead removal in aqueous solution. In: P. Yarlagadda, (Ed.), Proceedings of the 2015 4th International Conference on Sensors, Measurement and Intelligent Materials, 2016, pp. 1133-1136.
Zhang, H., et al., 2017a. Effect of feedstock and pyrolysis temperature on properties of biochar governing end use efficacy. Biomass and Bioenergy. 105, 136-146.
Zhang, M., et al., 2012. Synthesis of porous MgO-biochar nanocomposites for removal of phosphate and nitrate from aqueous solutions. Chemical Engineering Journal. 210, 26-32.
Zhang, P., et al., 2018a. Green and Size-Specific Synthesis of Stable Fe-Cu Oxides as Earth-Abundant Adsorbents for Malachite Green Removal. ACS Sustainable Chemistry & Engineering. 9229-9236.
Zhang, P., et al., 2017b. High efficiency removal of methylene blue using SDS surface-modified ZnFe2O4 nanoparticles. Journal of Colloid and Interface Science. 508, 39-48.
Zhang, Y., et al., 2018b. Biochar-supported reduced graphene oxide composite for adsorption and coadsorption of atrazine and lead ions. Applied Surface Science. 427, 147-155.
Zhang, Y., et al., 2019. Lead contamination in Chinese surface soils: Source identification, spatial-temporal distribution and associated health risks.
Zhao, B., et al., 2018. Effect of pyrolysis temperature, heating rate, and residence time on rapeseed stem derived biochar. Journal of Cleaner Production. 174, 977-987.
Zhou, N., et al., 2019. In situ modification provided by a novel wet pyrolysis system to enhance surface properties of biochar for lead immobilization. Colloids and Surfaces a-Physicochemical and Engineering Aspects. 570, 39-47.
Zhou, X. H., et al., 2018. Efficient removal of lead from aqueous solution by urea-functionalized magnetic biochar: Preparation, characterization and mechanism study. Journal of the Taiwan Institute of Chemical Engineers. 91, 457-467.
Zhu, L., Zhang, H., 2008. A novel method for the modification of zinc powder by ultrasonic impregnation in cerium nitrate solution. Ultrasonics Sonochemistry. 15, 393-401.
Zhu, L., et al., 2015. A study on chemisorbed oxygen and reaction process of Fe–CuOx/ZSM-5 via ultrasonic impregnation method for low-temperature NH3-SCR. Journal of Molecular Catalysis A: Chemical. 409, 207-215.

Graphical abstract

Synthesis of MgO-coated watermelon rind biochar

2. Filtration:
- Vacuum filtration to obtain $MgCl_2$ pretreated watermelon particles

4. Pyrolysis:
- Pyrolysis at designated temperatures

1 — 2 — 3 — 4 — 5

1. Mixing:
- Watermelon rind dry particles pretreated with excessive $MgCl_2$ at different concentrations

3. Drying:
- Oven dried at 80 ℃

5. Sieve:
- Sieved to ≤ 0.83 mm

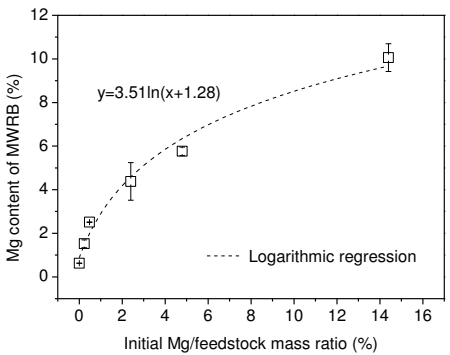

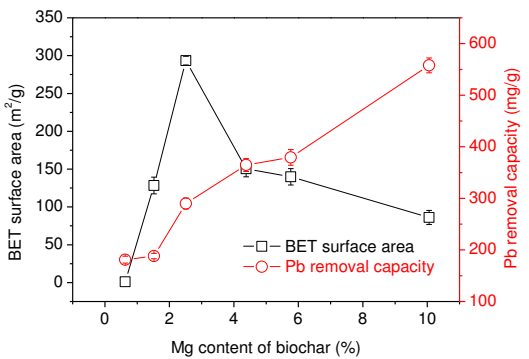

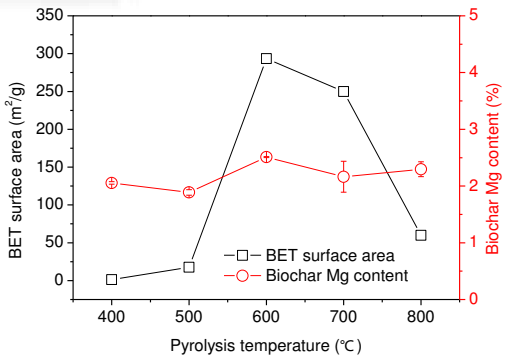

- **Coated Mg content vs Mg/feedstock ratio**
- **BET surface area vs coated Mg content**
- **Pb removal capacity vs coated Mg content**
- **BET surface area vs pyrolysis temperature**
- **Pb removal capacity vs pyrolysis temperature**

Supplementary Material

Click here to download Supplementary Material: Supporting information.docx